Shape from Photometric Ratio and Stereo*

KYOUNG MU LEE

Samsung Electronics Co., 416 Maetan-3 Dong, Paldal-Gu, Suwon City, Kyungki-Do, Korea, 441-742

AND

C.-C. JAY KUO

*Signal and Image Processing Institute and Department of Electrical Engineering Systems, University of Southern California,
Los Angeles, California 90089-2564*

Based on the traditional problem formulation, it is difficult to integrate the two important vision cues, i.e., shading and stereo, for shape reconstruction due to conflicting albedo and image projection assumptions. In this research, we propose a novel scheme to integrate shading and stereo. First, by using the photometric ratio, we derive a new SFS (shape from shading) formulation where no albedo is needed for shape reconstruction. Then, we establish a unified framework for the integration of photometric ratio and stereo by employing perspective projection on a parametric surface via minimizing a cost functional which consists of a weighted sum of shading and stereo errors. Simulation results are given to show the performance of our new robust algorithm. © 1996 Academic Press, Inc.

1. INTRODUCTION

Among many techniques for the reconstruction of a 3D shape of an object from its projected 2D images known as the "shape from X" problem, two modules, i.e., shape from shading (SFS) and geometric stereo method, have been considered the most important and have been studied intensively in the computer vision community for last several decades. Since the shading and stereo cues are inherently complementary depth information, attempts have been made by researchers to integrate these two information sources together for more robust and accurate shape reconstruction. Grimson [3] proposed to combine binocular shading and stereo data to determine the surface orientation along feature points of contours. Ikeuchi [6] reconstructed a depth map by using dual photometric stereo images and stereo region matching of the obtained surface orientations. Methods of combining stereo and shading

with a camera geometry transformation and by incorporating the stereo data as an initial estimate were investigated by Shao *et al.* [17] and Leclerc and Bobik [9], respectively. Recently, Cryer *et al.* [2] proposed a method based on a human visual model which integrates the low-frequency information from the stereo and high-frequency information from SFS.

However, there exist two major difficulties in their integration since the basic assumptions of the stereo method and the traditional SFS technique are conflicting. One is due to the albedo assumption of the object surface. The stereo method utilizes the feature of highly textured (varying albedo or color) surfaces so that the correspondence problem can be easily solved and a dense depth map can be obtained. In contrast, traditional SFS methods exploit the assumption of constant albedo across the entire surface; it is difficult to apply them to surfaces with varying albedo or multiple color. The other difficulty comes from the inconsistency of the projection model. The geometric stereo exploits the geometry of perspective projection, while most conventional SFS methods assume the simple orthographic projection model.

In this research, we propose a new method to integrate the depth information from the geometric stereo and shading in a single framework without any confliction. The main idea of our approach is to use the ratio of photometric stereo images to handle the varying albedo problem and employ a general parametric surface model under perspective projection to provide a unified geometric framework for the integration of the depth information sources. The integration is performed via a minimization procedure, where the cost functional consists of a weighted sum of square error terms corresponding to the photometric ratio and stereo depth error. We would like to point out that Wolff and Angelopoulou [18] also proposed an algorithm recently by combining stereo and shading information

based on photometric ratio. The main idea of their approach is to utilize the stereo pairs of photometric ratio values, instead of raw intensity values as considered in this work, for robust and accurate correspondence of the shape from stereo.

This paper is organized as follows. We briefly describe the general image formation model and the definition of the photometric ratio and reflectance ratio map in Section 2. The optical and geometrical properties of an ideal camera and a general parametric surface model are discussed in Section 3. The integration of depth source information is formulated as a minimization problem and the solution method is given in Section 4. Simulation results of the proposed algorithm and conclusion are presented in Sections 5 and 6, respectively.

2. PHOTOMETRIC RATIO

Due to the nature of the photometric invariance, the *photometric ratio* (or *reflectance ratio*) has been recently used as an important photometric feature for computer vision tasks such as object recognition, segmentation, and shape recovery [14, 18]. We briefly review the idea of photometric ratio and then derive the irradiance ratio equation which relates the photometric ratio, surface orientation, and illumination direction in this section.

It is known that the diffuse reflection of a smooth dielectric surface is not ideal Lambertian and can be modeled more accurately by direction [18].

$$L_r = \rho E_0 [1 - F(\mathbf{i}, \mathbf{n}, \eta)][1 - F(\mathbf{v}, \mathbf{n}, \eta)](\mathbf{i} \cdot \mathbf{n}), \quad (1)$$

where L_r is the reflected irradiance at a surface point, $F(\ )$ is the Fresnel reflection coefficient, ρ is the surface albedo, $\mathbf{n}$ is the surface normal, $\mathbf{i}$ and $\mathbf{v}$ are the vectors along the light source direction and viewer direction, and η is the refraction index of the dielectric surface. The image intensity value recorded by a sensor in an image plane through a lens system (see Fig. 1) can be described by the *lens collection* [5] with sensor gain g and bias b as
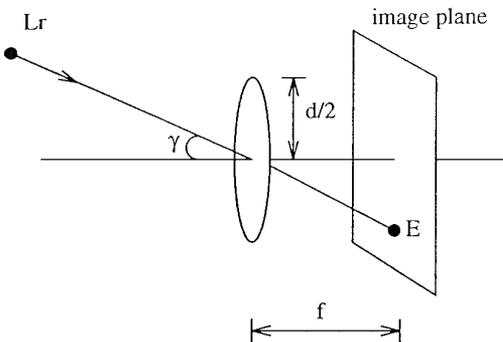
FIG. 1. Image formation through a lens system.

$$E = g \frac{\pi}{4} \left(\frac{d}{f} \right)^2 \cos^4 \gamma L_r + b, \quad (2)$$

where d is the lens diameter, f is the lens focal length, and γ is the angle of a ray from the object point to the center of the lens. The bias b usually comes from background noise and can be easily eliminated by calibrating the camera properly. Now, consider two photometric stereo images E_1 and E_2 without bias and taken under two different illumination directions $\mathbf{i}_1$ and i_2, respectively. By using (1) and (2), the ratio of the two intensity values corresponding to the same surface point with surface normal $\mathbf{n}$ can be written as

$$\tilde{E}_r = \frac{E_1}{E_2} = \frac{[1 - F(\mathbf{i}_1, \mathbf{n}, \eta)](\mathbf{i}_1 \cdot \mathbf{n})}{[1 - F(\mathbf{i}_2, \mathbf{n}, \eta)](\mathbf{i}_2 \cdot \mathbf{n})}.$$

Based on the observation that F is nearly constant until the incident angle $\theta = \cos^{-1}(\mathbf{i} \cdot \mathbf{n})$ approaches $90°$ for many surfaces [7], the above equation can be further simplified as

$$\tilde{E}_r = \frac{(\mathbf{i}_1 \cdot \mathbf{n})}{(\mathbf{i}_2 \cdot \mathbf{n})}.$$

Note however that the ratio E_1/E_2 may be unbounded. To make the concept computationally simple, we define a new photometric ratio function

$$E_r = \frac{1}{2} \left(1 + \frac{E_1 - E_2}{E_1 + E_2} \right) = \frac{(\mathbf{i}_1 \cdot \mathbf{n})}{(\mathbf{i}_1 \cdot \mathbf{n}) + (\mathbf{i}_2 \cdot \mathbf{n})},$$

which is bounded between 0 and 1.

Based on the above discussion, we obtain the following irradiance ratio equation relating the photometric ratio E_r and the reflectance ratio map R_r via

$$E_r(x, y) = R_r(\mathbf{n}), \quad (3)$$

where

$$E_r(x, y) = \frac{E_1(x, y)}{E_1(x, y) + E_2(x, y)}, \quad \text{and}$$

$$R_r(\mathbf{i}_1, \mathbf{i}_2, \mathbf{n}) = \frac{(\mathbf{i}_1 \cdot \mathbf{n})}{(\mathbf{i}_1 \cdot \mathbf{n}) + (\mathbf{i}_2 \cdot \mathbf{n})}. \quad (4)$$

With the two given light source directions $\mathbf{i}_1$ and $\mathbf{i}_2$, the reflectance ratio map R_r is only a function of the surface normal $\mathbf{n}$. It is independent of the surface albedo, camera characteristics, and viewing direction.
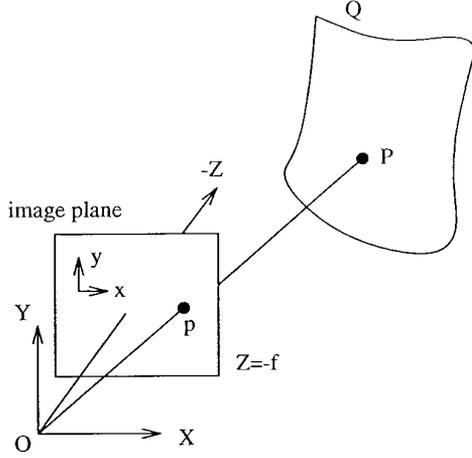
FIG. 2. Geometric model.

3. PERSPECTIVE PROJECTION ON A PARAMETRIC SURFACE

Consider a perspective image projection model as shown in Fig. 2, where the image plane $x - y$ is at $Z = -f$ and f is the focal length of a camera. The relationship between a surface point $\mathbf{P}(X, Y, Z)$ and the corresponding projected image point $\mathbf{p}(x, y, -f) \in \Omega$, where Ω is the image domain, can be written as

$$X(x, y) = -\frac{x}{f} Z(x, y), \quad \text{and} \quad Y(x, y) = -\frac{y}{f} Z(x, y). \quad (5)$$

Let us use $\mathbf{Q} = (X(x, y), Y(x, y), Z(x, y))$ to denote a parametric surface. By dividing the whole image domain Ω into simple subdomains, we can approximate $Z(x, y)$, which is projected to a certain submain, with a suitable approximating function. In general, the approximating function can be expressed as a linear combination of the individual element basis functions ϕ_i as

$$Z(x, y) = \sum_{i=1}^{M_n} Z_i \phi_i(x, y), \quad (6)$$

where Z_i are nodal variables and M_n is the total number of nodes. When the FEM (finite element method) is used in surface modeling, the image domain Ω is divided into triangles, parallelograms, or quadrilaterals, while linear, quadratic, or higher order polynomials can be used as the basis function [8, 16]. One commonly used example is the spline model, where a general uniform kth-order B-spline can be expressed as

$$Z(x, y) = \sum_{i=1}^{m} \sum_{j=1}^{n} V_{ij} N_{i,k}(x) N_{j,k}(y), \quad (7)$$

where V_{ij} is the control points in 2D notation and $N_{i,k}$ represents the kth-order basis function recursively determined via

$$N_{i,1}(t) = \begin{cases} 1, & \text{for } t_i \leq t \leq t_{i+1}, \\ 0, & \text{otherwise}, \end{cases}$$

and

$$N_{i,k}(t) = \frac{(t - t_i)}{(t_{i+k-1} - t_i)} N_{i,k-1}(t) + \frac{(t_{i+k} - t)}{(t_{i+k} - t_{i+1})} N_{i+1,k-1}(t).$$

Note that by ordering the 2D nodal indices (i, j) into a 1D index sequence, (7) can be represented in a form given by (6).

One can use the vector calculus to determine the surface normal $\mathbf{n}$ as

$$\mathbf{n} = \frac{\partial \mathbf{Q}}{\partial x} \times \frac{\partial \mathbf{Q}}{\partial y} = \begin{vmatrix} \mathbf{i} & \mathbf{j} & \mathbf{k} \\ \dfrac{\partial \mathbf{X}}{\partial x} & \dfrac{\partial \mathbf{Y}}{\partial x} & \dfrac{\partial \mathbf{Z}}{\partial x} \\ \dfrac{\partial \mathbf{X}}{\partial y} & \dfrac{\partial \mathbf{Y}}{\partial y} & \dfrac{\partial \mathbf{Z}}{\partial y} \end{vmatrix}. \quad (8)$$

By substituting (5) and (6) into (8), we have

$$\mathbf{n} = \begin{bmatrix} \dfrac{1}{f} Z \dfrac{\partial \mathbf{Z}}{\partial x} \\ \dfrac{1}{f} Z \dfrac{\partial \mathbf{Z}}{\partial y} \\ \dfrac{Z}{f^2} \left(Z + x \dfrac{\partial \mathbf{Z}}{\partial x} + y \dfrac{\partial \mathbf{Z}}{\partial y} \right) \end{bmatrix}$$

$$= \frac{1}{f^2} \begin{bmatrix} f \sum_{i=1}^{M_n} \sum_{j=1}^{M_n} Z_i Z_j \phi_i \dfrac{\partial \phi_j}{\partial x} \\ f \sum_{i=1}^{M_n} \sum_{j=1}^{M_n} Z_i Z_j \phi_i \dfrac{\partial \phi_j}{\partial y} \\ \sum_{i=1}^{M_n} \sum_{j=1}^{M_n} Z_i Z_j \left(\phi_i \phi_j + x \phi_i \dfrac{\partial \phi_j}{\partial x} + y \phi_i \dfrac{\partial \phi_j}{\partial y} \right) \end{bmatrix}. \quad (9)$$

It is worthwhile to point out from the above expression that, given the camera focal length f and a suitable interpolating function ϕ, the normal vector $\mathbf{n}$ at a surface point corresponding to an image point $(x, y, -f)$ is parameterized by the nodal variables Z_i, $i = 1, \ldots, M_n$. Therefore, by using (9), we can represent the reflectance ratio map R_r in (4) with the surface nodal variables so that the right-
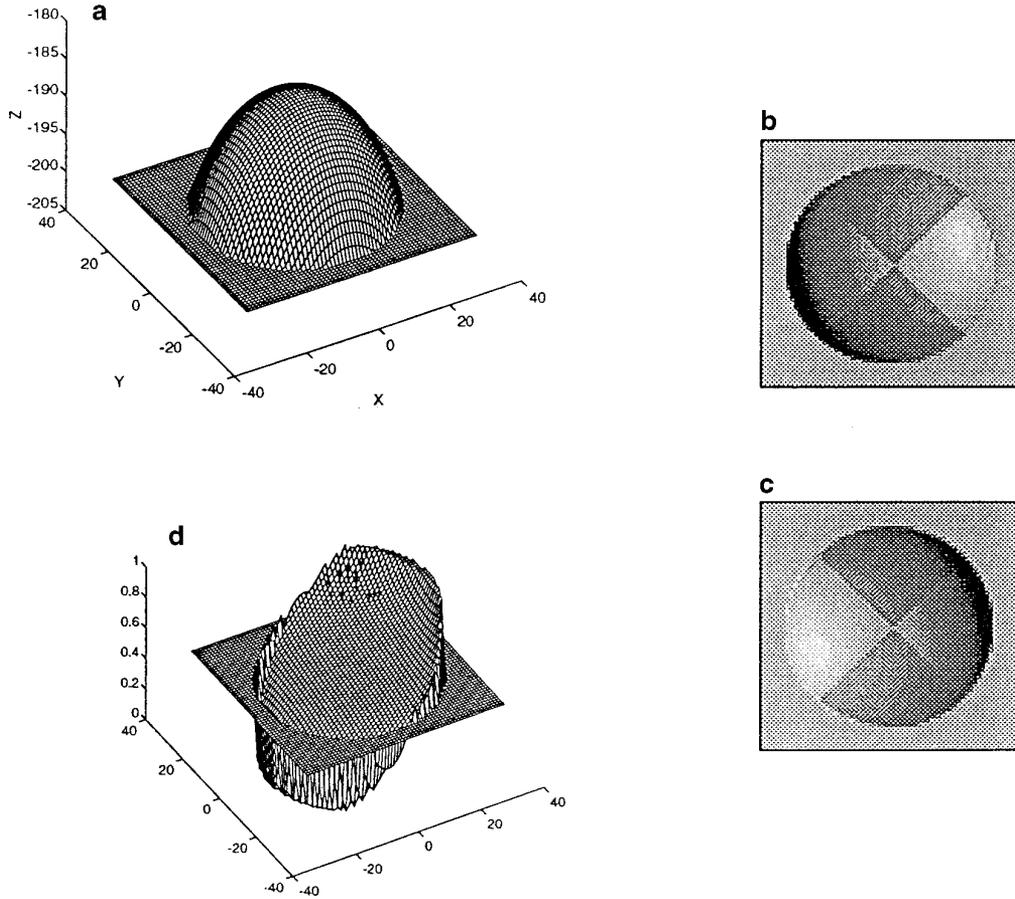
FIG. 3. The spherical surface test problem: (a) the ground truth of the spherical surface with varying albedo; two synthetic Lambertian textured images illuminated with (b) (tilt, slant) = (20°, 40°) and (c) (tilt, slant) = (200°, 40°); and (d) the 3-plot of the corresponding photometric ratio values.

hand side of the image irradiance equation (3) is discretized and parameterized in terms of Z_i, $i = 1, \ldots, M_n$, i.e.,

$$E_r(x, y) = R_r(Z_1, \ldots, Z_{M_n}). \tag{10}$$

4. COMBINING SHADING AND STEREO DEPTH INFORMATION

In general, the geometric stereo provides sparse depth information at the feature points where the albedo varies rapidly on the object surface. Most of the stereo methods can be classified into two groups, i.e., feature-based methods [1, 12] and area-based methods [13, 4]. The feature-based technique attempts to find correspondence of sparse and more abstract features such as edgels or segments, while the area-based technique tries to find matches of features such as intensity at each pixel or the correlation of a local window of intensities. Let us assume that we have depth information at some feature points obtained by suitable stereo method, and denote the depth data as

$d(x_m, y_m), m = 1, \ldots, M_d$, where M_d is the total number of the data point. Then, surface reconstruction by integrating photometric ratio and stereo depth cues comes to determine the surface nodal parameters Z_i, $i = 1, \ldots, M_n$, which satisfy following system of equations simultaneously:

$$E_r(x, y) - R_r(Z_1, \ldots, Z_{M_n}) = 0,$$
$$Z(x_m, y_m) - d(x_m, y_m) = 0, \quad m = 1, \ldots, M_d. \tag{11}$$

Usually, the number of unknown M_n is less than the number $M_d + 1$ of equations so that the system is overdetermined and can be solved by the least-squares method. That is, one natural way to combine the photometric ratio information and the depth information obtained by geometric stereo method is to minimize the cost functional

$$\mathcal{E} = \mathcal{E}_r + \mathcal{E}_d, \tag{12}$$

where $\mathcal{E}_r$ and $\mathcal{E}_d$ are the square error terms corresponding

the photometric ratio and the stereo data, respectively. They are represented as

$$\mathcal{E}_r = \int\int_\Omega (E_r(x, y) - R_r(x, y))^2 \, dx \, dy$$

$$= \int\int_\Omega (E_r(x, y) - R_r(Z_1, \ldots, Z_{M_n}))^2 \, dx \, dy,$$

$$\mathcal{E}_d = \int\int_\Omega w(x, y)(Z(x, y) - d(x, y))^2 \, dx \, dy$$

$$= \int\int_\Omega w(x, y)\left(\sum_{j=1}^{M_n} Z_j\phi_j(x, y) - d(x, y)\right)^2 \, dx \, dy,$$

(13)

where $Z(x, y)$ is the estimated height, $d(x, y)$ is the depth value at point (x, y) obtained from stereopsis, and $w(x, y)$ is a weighting function. If no height data are available at point (x, y), we choose $w(x, y) = d(x, y) = 0$.

The standard nonlinear optimization methods such as the Newton–Raphson method and the Levenberg–Marquardt method can be used for minimizing (12) [15]. In this research, we employ a simple effective method called the successive linearization method in which the nonlinear function R_r is linearized with respect to the nodal variables Z_i successively so that (12) can be solved by linear least squares. We outline the procedure below. For implementation details, see [10, 11].

The successive linearization of R_r can be accomplished by the Taylor series expansion. Suppose that we have an estimated solution $\mathbf{Z}^{n-1} = (Z_1^{n-1}, Z_2^{n-1}, \ldots, Z_{M_n}^{n-1})^T$ at $(n-1)$th iteration, then the approximated reflectance map ratio at nth iteration becomes

$$R_r(x, y) \approx \sum_{i=1}^{M_n} \alpha_i(x, y)Z_i^n + \xi^n(x, y), \qquad (14)$$

where

$$\alpha_i(x, y) = \left.\frac{\partial R_r(x, y, Z_1, \ldots, Z_{M_n})}{\partial Z_i}\right|_{(Z_1^{n-1}, \ldots, Z_{M_n}^{n-1})},$$

and

$$\xi^n(x, y) = R_r(x, y, Z_1^{n-1}, \ldots, Z_{M_n}^{n-1}) - \sum_{i=1}^{M_n} \alpha_i(x, y)Z_i^{n-1}.$$

By substituting (14) into (13) and rearranging it, we can represent $\mathcal{E}_r$ in matrix form as

$$\mathcal{E}_r = \frac{1}{2}(\mathbf{Z}^n)^T\mathbf{A}^n\mathbf{Z}^n - (\mathbf{b}^n)^T z + C_r^n$$

and express the stereo data term in (13) as

$$\mathcal{E}_d = \frac{1}{2}(\mathbf{Z}^n)^T\Phi\mathbf{Z}^n - \mathbf{h}^T z + C_d,$$

where the element of matrices $\mathbf{A}$ and Φ, and vectors $\mathbf{b}$ and $\mathbf{h}$ are

$$\mathbf{A}_{ij}^n = \int\int_\Omega \alpha_i(x, y)\alpha_j(x, y) \, dx \, dy,$$

$$\mathbf{b}_i^n = \int\int_\Omega \alpha_i(x, y)(E_r(x, y) - \xi^n(x, y)) \, dx \, dy.$$

$$\Phi_{ij} = \int\int_\Omega w(x, y)\phi_i(x, y)\phi_j(x, y) \, dx \, dy,$$

$$\mathbf{h}_i = \int\int_\Omega w(x, y)d(x, y)\phi_i(x, y) \, dx \, dy.$$
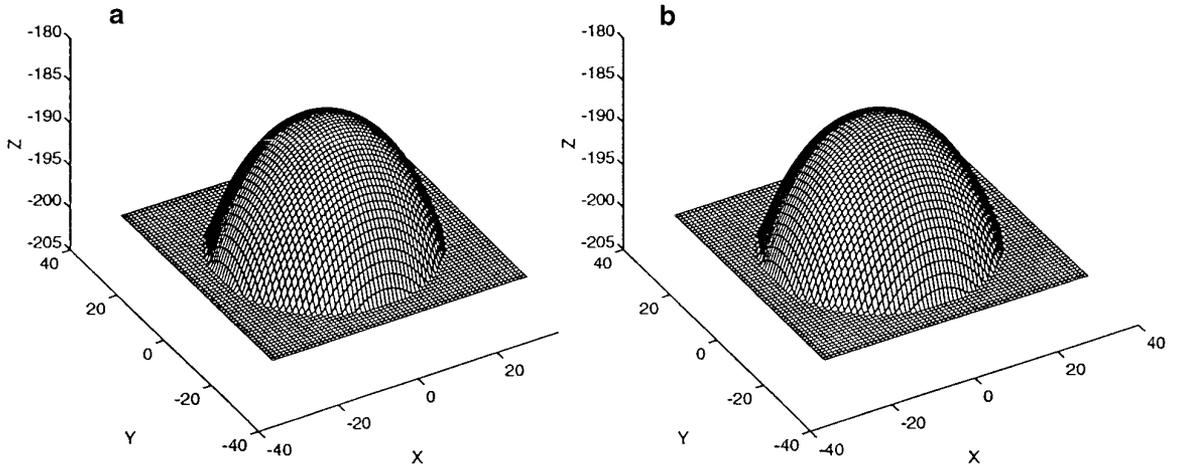
FIG. 4. Reconstructed surfaces with: (a) photometric ratio information only ($\Delta\tau = 180°$); (b) combined stereo and photometric ratio information ($\Delta\tau = 180°$).
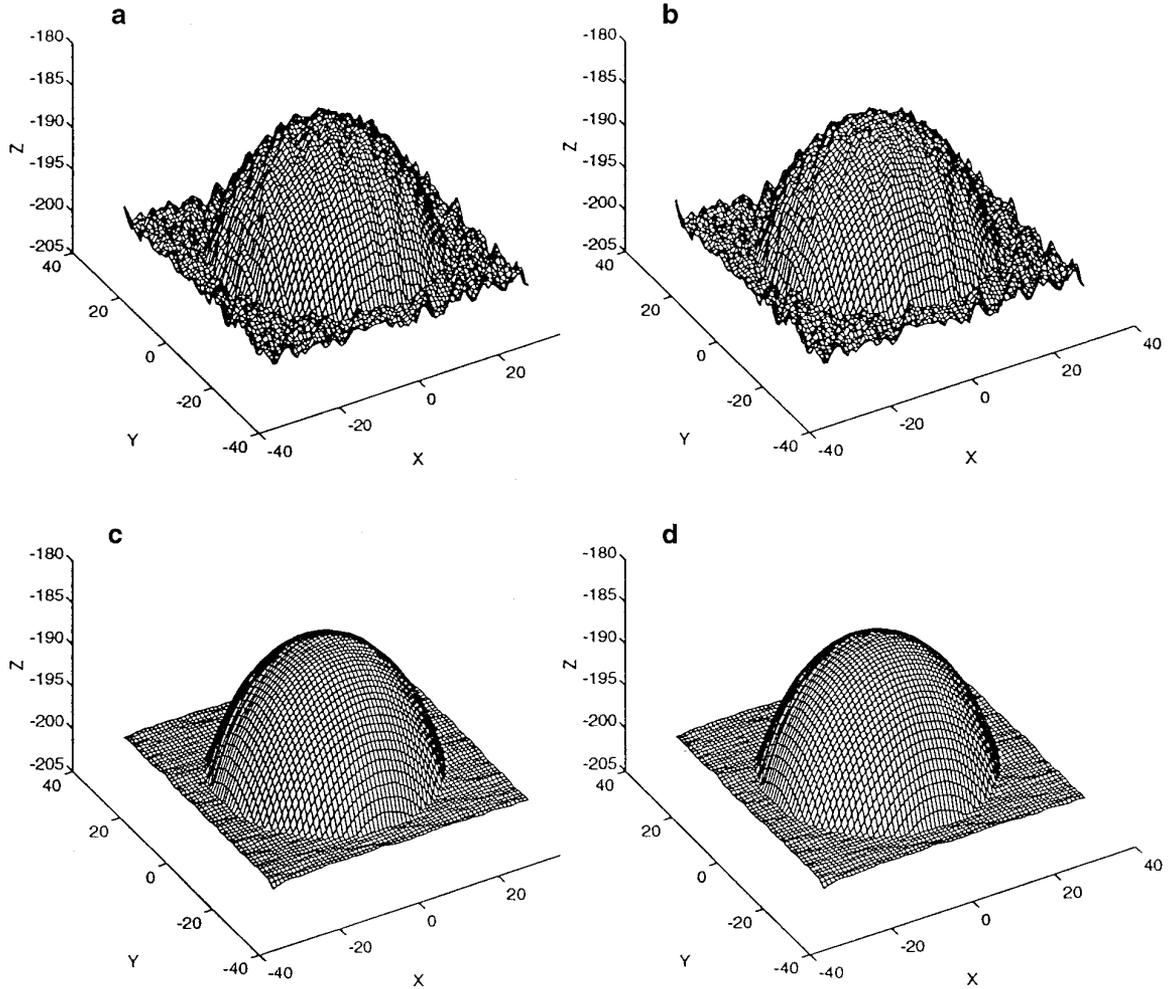
FIG. 5. Reconstructed surfaces with: (a) noise-corrupted photometric ratio ($\Delta\tau = 30°$); (b) combined stereo and noise-corrupted photometric ratio ($\Delta\tau = 30°$); (c) noise-corrupted photometric ratio ($\Delta\tau = 180°$); and (d) combined stereo and noise-corrupted photometric ratio ($\Delta\tau = 180°$).

Therefore, the overall cost functional can be represented as

$$\mathscr{E} = \frac{1}{2}(\mathbf{Z}^n)^T \mathbf{M}^n \mathbf{Z}^n - (\mathbf{m}^n)^T \mathbf{Z}^n + C^n, \qquad (15)$$

where $M = \mathbf{A}^n + \Phi$, $\mathbf{m} = \mathbf{b}^n + \mathbf{h}$, and $C^n = C_r^n + C_d$. The minimization of the quadratic functional in (15) with respect to the nodal variables $\mathbf{Z}^n$ is equivalent to the solution of the following linear system of equations:

$$\mathbf{M}^n \mathbf{z}^n = \mathbf{m}^n.$$

Since the stiffness matrix $\mathbf{M}^n$ is sparse and symmetric, the system can be efficiently solved by iterative linear solvers. The successive linearization scheme starts with an arbitrary initial estimate z^0 and iteratively refines the surface until it satisfies a termination criterion.

5. EXPERIMENTAL RESULTS

In this section, we present some simulation results to demonstrate the performance of the proposed algorithm. A simple linear model with triangular subdomains is used for the surface approximation in this test. The test object is a spherical surface as shown in Fig. 3a, where two different albedo values are assigned to the surface to generate synthetic Lambertian textured images. A pair of photometric stereo images are generated by illuminating from the directions of (*tilt, slant*) = (20°, 40°) and (200°, 40°) as shown in Figs. 3b and 3c. Figure 3d shows the 3D plot of the photometric ratio values of Figs. 3b and 3c which are determined via (4). The focal length of the camera f is set to 100. The depth values along the texture boundaries are determined with synthesized geometric stereo images and used as the stereo depth constraint throughout the test.

First, we tested the effect of relative illumination direc-

6. CONCLUSION

In this work, we propose a new algorithm to integrate depth sources from shading and stereo depth information. By utilizing the ratio of two photometric stereo images of an object, we eliminate the varying albedo and camera characteristic problem for the SFS. Moreover, by employing a perspective projection model, we establish a common geometrical and optical framework for both SFS and stereopsis so that the depth information from stereo can be readily integrated with that from shading. By introducing a parametric surface model, we approximate the surface with a linear combination of suitable basis functions and discretize and parameterize the photometric ratio irradiance equation with the nodal depth coefficients. The integration of photometric ratio (shading) and stereo information is obtained by considering an objective functional as a weighted sum of stereo depth and photometric ratio components. We then reconstruct the surface directly by determining all nodal depth variables through a minimization process of the objective functional. Our algorithm refines the reconstructed surface iteratively by applying a successive linearization scheme to the nonlinear reflectance map.

TABLE 1

The RMS Error of the Reconstructed Surface Depth Values with Various Tilt Angle Differences ($\Delta \tau = \|\tau_2 - \tau_1\|$) of the Two Light Sources

$\Delta\tau$ (°)	PR	PR + stereo	PR (w/noise)	PR (w/noise) + stereo
30	0.0020	0.0009	0.3601	0.3546
60	0.0015	0.0003	0.2425	0.2135
90	0.0009	0.0002	0.1340	0.1307
120	0.0004	0.0001	0.1201	0.1084
150	0.0002	0.0001	0.1238	0.1044
180	0.0001	0.0001	0.0740	0.0695

Note: PR = photometric ratio.

tions of the two light sources for several cases in which a single photometric ratio, combined stereo depth, and photometric ratio as well as the noise added photometric stereo information are used for the reconstruction. We observed that the accuracy of the reconstructed surface is less dependent on the slant angles while it is heavily affected by the tilt angles. The RMS error of the reconstructed surfaces with respect to the relative difference of the tilt angles, ($\Delta\tau = \|\tau_2 - \tau_1\|$) of the two light sources are summarized in Table 1. The first column represents the difference of the tilt angles, and the second and third columns show the corresponding RMS errors when the photometric ratio only and the combined photometric ratio and stereo depth constraints are used for the reconstruction, respectively. The RMS errors for the case where photometric stereo images are corrupted by 5% random noise are shown in the fourth and fifth columns. One can conclude from these results that the reconstruction error is minimized when the two light sources are opposite in their tilt angles, i.e., $\Delta\tau = 180°$ and it becomes larger as they are closer to each other.

Figures 4a and 4b show the reconstructed results by using single photometric ratio information and combined stereo and photometric ratio with $\Delta\tau = 180°$, respectively. Both results are quite accurate and almost perfect reconstruction has been achieved as indicated by the reconstruction error in the last rows of the second and third columns of Table 1. To demonstrate the robustness of the algorithm against noise, we tested it with photometric stereo images corrupted with 5% random noise. The recovered surfaces by using photometric ratio only and combined depth cues for both $\Delta\tau = 30°$ and 180° are shown in Figs. 5a–5d, and the corresponding reconstruction error of those surfaces are shown in the first and the last rows of fourth and fifth columns of Table 1. We see from these results that the photometric ratio is insensitive to the noise and produces a relatively good reconstructed surfaces, especially when the two light sources are opposite in their tilt angles, i.e., ($\Delta\tau = 180°$).

REFERENCES

1. S. Barnard and W. Thompson, Disparity analysis of images, *IEEE Trans. Pattern Anal. Machine Intell.* **2,** 1980, 333–340.

2. J. E. Cryer, P. S. Tsai, and M. Shah, "Combining Shape from Shading and Stereo Using Human Visual Model," Tech. Rep. CS-TR-92-25, Central Florida, 1992.

3. W. E. L. Grimson, Binocular shading and visual surface reconstruction, *Comput. Vision Graphics Image Process.* **28,** 1984, 19–43.

4. M. J. Hannah, SRI's baseline stereo system, in *DARPA Image Understanding Workshop, Miami, Florida, December 1985,* pp. 149–155.

5. B. K. P. Horn, *Robot Vision,* Cambridge, MA: MIT Press, 1986.

6. K. Ikeuchi, Reconstructing a depth map from intensity maps, in *IEEE International Conference on Pattern Recognition, Montreal, Canada, August 1984,* pp. 736–738.

7. K. Ikeuchi and K. Sato, Determining reflectance properties of an object using range and brightness images, *IEEE Trans. Pattern Anal. Machine Intell.* **13**(11), 1991, 1139–1153.

8. C. Johnson, *Numerical Solutions of Partial Differential Equations by the Finite Element Method,* Cambridge, UK: Cambridge Univ. Press, 1987.

9. Y. G. Leclerc and A. F. Bobick, The direct computation of height from shading, in *IEEE Conference on Computer Vision and Pattern Recognition, Hawaii, May 1991,* pp. 552–558.

10. K. M. Lee and C.-C. J. Kuo, Shape from shading with a linear triangular element surface model, *IEEE Trans. Pattern Anal. Machine Intell.* **15,** 1993, 815–822.

11. K. M. Lee and C.-C. J. Kuo, Surface reconstruction from photometric stereo images, *J. Optical Soc. Amer. A* **10,** 1993, 855–868.

12. H. S. Lim and T. O. Binford, Structural correspondence in stereo vision, in *DARPA Image Understanding Workshop, Cambridge, Massachusetts, April 1988,* pp. 794–808.

13. K. Mori, M. Kidode, and H. Asada, An iterative prediction and correction method for automatic stereo comparison, *Comput. Graphics Image Process.* **2,** 1973, 393–401.

14. S. K. Nayar and R. M. Bolle, Object recognition based on reflectance and geometry, in *Proceedings of SPIE Conference: Geomeric Methods in Computer Vision II, San Diego, California, July 1993,* Vol. 2031.

15. W. H. Press, B. P. Flannery, S. A. Teukolsky, and W. T. Vetterling, *Numerical Recipes in C,* Cambridge, UK: Cambridge Univ. Press, 1988.

16. H. R. Schwartz, *Finite Element Methods,* San Diego: Academic Press, 1988.

17. M. Shao, R. Chellappa, and T. Simchony, Reconstructing a 3-D depth map from one or more images, *Comput Vision Graphics Image Process. Image Understanding.* **53,** 1991, 219–226.

18. L. B. Wolff and E. Angelopoulou, 3D stereo using photometric ratios, in *Proceedings of SPIE Conference: Optics, Illumination, and Image Sensing for Machine Vision VIII, Boston, MA, September 1993,* Vol. 2065.

DR. KYOUNG MU LEE received B.S. and M.S. degrees in control and instrumentation engineering from the Seoul National University, Seoul, Korea in 1984 and 1986, respectively, and a Ph.D. degree in electrical engineering from the University of Southern California in 1993. From 1993 to 1994, he worked as a research associate in the Signal and Image Processing Institute at the University of Southern California. Since April 1994, he has been with Samsung Electronics Co., Ltd. in Korea, where he is currently a senior researcher. His research interests include computer vision, image processing, and multimedia applications.

DR. C.-C. JAY KUO received a B.S. degree from the National Taiwan University, Taipei, in 1980 and M.S. and Ph.D. degrees from the Massachusetts Institute of Technology, Cambridge, in 1985 and 1987, respectively, all in Electrical Engineering. From October 1987 to December 1988, he was Computational and Applied Mathematics (CAM) Research Assistant Professor in the Department of Mathematics at the University of California, Los Angeles. Since January 1989, he has been with the Department of Electrical Engineering Systems and the Signal and Image Processing Institute at the University of Southern California, where he currently has a joint appointment as Associate Professor of Electrical Engineering and Mathematics. His research interests are in the areas of digital signal and image processing, wavelet theory and applications, video image compression, multimedia, and large-scale scientific computing. He has more than 160 technical publications appearing in journals and conferences. Dr. Kuo is a member of Sigma Xi, SIAM, SPIE, and ACM and is a Senior Member of IEEE. He serves as Associate Editor for *IEEE Transaction on Image Processing* and *IEEE Transaction on Circuits and Systems: Video Technology* and is on the editorial board of the *Journal of Visual Communication and Image Representation.* Dr. Kuo received the National Science Foundation Young Investigator Award (NYI) and Presidential Faculty Fellow (PFF) Award in 1992 and 1993, respectively.